J Solid State Electrochem (2016) 20:3315–3322
DOI 10.1007/s10008-016-3353-x

ORIGINAL PAPER

Direct electrochemistry and electrocatalysis of cytochrome *c* based on dandelion-like Bi_2S_3 nanoflowers

Qinglin Sheng[1] · **Yu Shen**[1] · **Qian Wu**[1] · **Jianbin Zheng**[1]

Received: 17 November 2015 / Revised: 14 July 2016 / Accepted: 31 July 2016 / Published online: 14 August 2016

Abstract The direct electrochemistry and electrocatalysis of cytochrome *c* (Cyt *c*) based on dandelion-like bismuth sulfide (*d*-Bi_2S_3) nanoflowers have been developed. The morphologies and composition of the *d*-Bi_2S_3 were characterized by scanning electron microscopy (SEM), transmission electron microscopy (TEM), and energy dispersive X-ray spectroscopy (EDS). Then, the electrochemical behaviors of Cyt *c* immobilized within the d-Bi_2S_3/chitosan film and its electrocatalytic ability toward hydrogen peroxide (H_2O_2) reduction were investigated by cyclic voltammetry. The electron transfer rate constant was estimated to be 13.1 s^{-1}, suggesting that a fast direct electron transfer was realized. The prepared Cyt *c*/*d*-Bi_2S_3/chitosan nanobiocomposite-modified electrode possessed excellent electrocatalytic ability toward H_2O_2 reduction that showed linearity in the range from 0.5 μM to 1.56 mM with a correlation coefficient of 0.9993. The detection limit was 0.2 μM on signal-to-noise ratio of 3. In addition, the *d*-Bi_2S_3 nanoflowers may be also applied to direct electron transfer of other redox proteins.

Keywords Direct electrochemistry · Cytochrome *c* · Bismuth sulfide · Hydrogen peroxide

Introduction

The research on direct electron transfer between redox proteins and electrode surfaces is of great importance in electron transfer mechanism study of biomolecule and biosensor construction [1–3]. In recent decades, the emerging desires for new materials with good biocompatibility and fast electron transfer rate have attracted enormous attention since the redox centers of redox proteins are always buried deeply and the proteins are easy to be irreversibly denatured after immobilized on electrode surfaces.

Among various kinds of redox proteins, cytochrome *c* (Cyt *c*) is considered to be one of the most ideal and important heme proteins due to its well-known structure, commercial availability, and important function in the biological process. Moreover, nanomaterials are always employed as effective supporter for redox protein immobilization and direct electrochemistry [4–6]. To date, many kinds of nanomaterials have been used for the direct electrochemistry of Cyt *c* [7–12]. For instance, a kind of composite film made of layer-by-layer assembled ordered mesoporous carbon nanospheres and poly(diallyldimethylammonium) was used as a biocompatible matrix for Cyt *c* immobilization [9]. Based on the biocompatible matrix, a novel hydrogen peroxide (H_2O_2) biosensor with high sensitivity, wide linear range, and low detection limit was proposed. It was also reported that the combination of graphene oxide with multiwalled carbon nanotube was employed for Cyt *c* immobilization and biosensor fabrication [10]. The results revealed that the formation of a highly conducting MWCNT network on the graphene oxide surface could improve the selectivity for H_2O_2 sensing exceptionally in the presence of high concentration interferents. More recently, silicon nanomaterials with porous cavities were found to retain the Cyt *c*'s redox activity even after several months of its immobilization and showed high electrochemical stability [11]. Another example was the incorporation of Cyt *c* with three-dimension porous calcium alginate to realize the direct electrochemistry of Cyt *c* [12]. Thus, it is expected that using three-dimensional structures of nanomaterials is one of the most effective ways for protein immobilization and direct electron transfer.

✉ Jianbin Zheng
zhengjb@nwu.edu.cn

[1] Institute of Analytical Science/Shaanxi Provincial Key Laboratory of Electroanalytical Chemistry, Northwest University, Xi'an, Shaanxi 710069, China

Semiconductor nanomaterials have driven a hot trend in optical and electronic devices [13–15]. Moreover, they are considered to be biocompatible immobilization matrices as well as nanoscaled electrical wires for redox-active molecules [16–20]. As was reported, a fast electron transfer rate was achieved by electrostatic interaction composition of water soluble CdS/Mn nanoparticles immobilized hemoglobin [21]. An *L*-cysteine capped cadmium sulfide-chitosan nanocomposite, which could also strongly adsorb hemoglobin, and the as-prepared biosensor exhibited excellent bioelectrocatalysis for H_2O_2 reduction [22]. Bismuth sulfide (Bi_2S_3), which is a perfect semiconducting main-group metal chalcogenide with a direct energy band gap ranging from 1.2 to 1.7 eV, has also attracted considerable attention in the electrochemical sensing field. For example, Bi_2S_3 with rod-like and cauliflower-like morphologies exhibited electrocatalytical abilities for antipyrine and ascorbic acid oxidation [23, 24]. More recently, Zhu et al. prepared polyaniline-Bi_2S_3 nanocomposite for DNA immobilization and developed a sensitive impedimetric DNA biosensor with a detection limit of 4.37×10^{-16} M [20]. Thus, it could be expected that the nanostructure Bi_2S_3 combined with redox proteins is promising to create unique materials and open up new opportunities for bioelectrochemistry studies. In this work, we describe the preparation of dandelion-like bismuth sulfide (*d*-Bi_2S_3) nanoflowers and direct electrochemistry of Cyt *c* immobilized on the *d*-Bi_2S_3 composite matrix. The electrochemical behaviors and electrocatalytic ability toward H_2O_2 reduction of the composite film are thoroughly investigated by electrochemical methods.

Experimental

Reagents

$BiCl_3$ and acetothioamide were purchased from Aladdin Reagent Co., Ltd., Shanghai (China). Cyt *c* was purchased from Sigma and used without further purification. Chitosan (CHIT) (MW 1×10^6, >90 % deacetylation) was purchased from Shanghai Xiangsheng Biotechnology Co., Ltd. (China). Thirty percent aqueous H_2O_2 solution was purchased from Shanghai Chemical Plant Co., Ltd. The diluted solutions with desired concentration used in the experiments were freshly prepared. All solutions were prepared with ultrapure water (>18 MΩ cm) obtained from a Millipore Milli-Q water purification system.

Apparatus

Scanning electron microscopic (SEM) measurements were carried out on a scanning electron microscope (JEOL JSM–6700F) at 15 kV. Transfer electron microscopy (TEM) was acquired with a JEOL JEM-3010 high-resolution transmission electromicroscope using an accelerating voltage of 150 kV. TEM images were obtained at different parts of the grid and with different magnifications. The energy dispersive spectrometric (EDS) analysis of the *d*-Bi_2S_3 was also performed during the SEM measurements. UV–vis spectra were recorded on a Shimadzu UV–2501PC spectrophotometer. The circular dichroism (CD) measurements were carried out with a CD spectrometer J700 (JASCO) using a quartz cell with a path length of 1.0 cm. The protein-adsorbed slides were placed manually, perpendicular to the light path. Each CD spectrum was the average of three scans.

A model CHI660D electrochemistry workstation (Shanghai Chenhua Instruments Co. Ltd., China) was employed for all the electrochemical techniques. A conventional three-electrode system was used. The prepared electrode was used as the working electrode. A standard saturated calomel electrode (SCE) and a platinum wire electrode were served as the reference electrode and the auxiliary electrode, respectively. All the electrochemical experiments were conducted at room temperature. Electrolyte solutions were purged with highly purified nitrogen for at least 20 min prior to experiments. A nitrogen atmosphere was then kept over solutions in the cell.

Synthesis of *d*-Bi_2S_3

In a typical synthesis, 31.5 mg of $BiCl_3$ and 15.3 mg of acetothioamide were firstly dissolved in 3 mL deionized water. Then, 2 mL 1-butyl-3-methylimidazolium tetrafluoroborate ([BMIM][BF_4]) was added into the above solution. After vigorous magnetic stirring, the mixture solution was transferred into a stainless autoclave and heated at 120 °C for 6 h. After cooling to room temperature naturally, the black precipitates were collected and washed with distilled water and proof ethanol, respectively, for three times.

Fabrication of the composite film-modified electrodes

Prior to use, a glassy carbon electrode (GCE) was polished by a polishing cloth with alumina of successively smaller particles (0.3 and 0.05 μm diameter), then rinsed with water, and ultrasonicated in ethanol and ultrapure water, respectively. Typically, 1.0 mg *d*-Bi_2S_3 was dispersed in 0.5 mL of CHIT solution with the help of ultrasonic agitation. Then, 2 mg of Cyt *c* was added into the above solution. The mixture was hand-mixed completely and was allowed to be left for overnight at 4 °C in a refrigerator. Then 6 μL of the above solutions was cast onto the surface of a polished GCE (3 mm diameter) by using a syringe to prepare the Cyt *c*-*d*-Bi_2S_3/CHIT/GCE. The electrode was stored at 4 °C in a refrigerator when not in use. A 0.1 M H 7.0 sodium phosphate-buffered (PB) solution was used in all electrochemical studies unless

otherwise stated. Electrolyte solutions were purged with highly purified nitrogen for at least 20 min prior to experiments. A nitrogen atmosphere was then kept over solutions in the cell. For comparison with Cyt *c*-*d*-Bi_2S_3/CHIT/GCE, *d*-Bi_2S_3/CHIT/GCE, Cyt *c*/CHIT/GCE and CHIT/GCE were prepared with similar procedures as described above.

Results and discussion

Characterization of *d*-Bi_2S_3 and Cyt *c*-*d*-Bi_2S_3

The morphology of the as-synthesized products was first characterized by SEM. As shown in Fig. 1a, a uniform *d*-Bi_2S_3 nanoflower with the outer diameter of about 6 μm was obtained. Figure 1b shows the TEM image of *d*-Bi_2S_3 nanostructures. The typical nanorod within the *d*-Bi_2S_3 nanostructures was about 50 nm in width and 1 mm in length. The magnified TEM image shown in Fig. 1c reveals the circumstantiality of some individual Bi_2S_3 nanorods that have a smooth surface and uniform diameter along its entire length. Moreover, the elemental analysis with EDS was also employed to analyze the chemical composition of *d*-Bi_2S_3 nanoflower. As shown in Fig. 1d, no peaks of impurities related to other elements were detected, revealing the high purity of the as-synthesized samples. The Au peaks observed from the spectrum were the gold layer sputtered for SEM in order to enhance their conductivity of Bi_2S_3. The atomic ratio of Bi/S is approximately 2:3, which is in good agreement with the stoichiometric ratio of the Bi_2S_3. After immobilization of Cyt *c*-*d*-Bi_2S_3 with CHIT by drop casting, the morphology of *d*-Bi_2S_3 on electrode surface showed a smoother surface (Fig. 1e), suggesting the immobilization of Cyt *c* within the *d*-Bi_2S_3-CHIT film. The surface density of *d*-Bi_2S_3 nanocrystals immobilized onto the electrode surface was about 2×10^4 nanocrystals per square millimeter calculated from the SEM results. The XRD pattern of the *d*-Bi_2S_3 nanoflower was also recorded. From Fig. 2, it can be seen that the characteristic peaks are strong and sharp, suggesting a highly crystalline nature of the *d*-Bi_2S_3. The positions of the peaks are in good conformity with those of the crystal structure of Bi_2S_3 and can be indexed to orthorhombic Bi_2S_3 (JCPDS 17-0320). Moreover, no peaks from impurities were observed, indicating a high purity of the *d*-Bi_2S_3 nanoflower.

To qualitatively investigate the biological activity of Cyt *c* immobilized on *d*-Bi_2S_3/CHIT composite film, UV–vis spectra of Cyt *c* and Cyt *c*-*d*-Bi_2S_3/CHIT were recorded, which could monitor the Soret band of Cyt *c* before and after immobilization. Figure 3a shows the UV–vis spectra of Cyt *c* and Cyt *c*-*d*-Bi_2S_3/CHIT, respectively. As shown in curve a, three characteristic peaks located at 408, 522, and 548 nm [25] can be ascribed to the Soret, α, and β bands associated with the porphyrin ring, respectively. After immobilization, the characteristic absorption peaks for Cyt *c*-*d*-Bi_2S_3/CHIT composites in curve b are almost the same as that of free Cyt *c*, demonstrating that Cyt *c* in the *d*-Bi_2S_3/CHIT composite film retained its near native conformation. Since protein structures are dynamic and susceptible to operational conditions and environment, CD spectra of native Cyt *c* and Cyt *c*-*d*-Bi_2S_3 were recorded to evaluate the secondary structure in terms of α-helix, β-sheet, and unordered forms of the polypeptide chain [26]. As shown in Fig. 3b, the trends of the two spectra

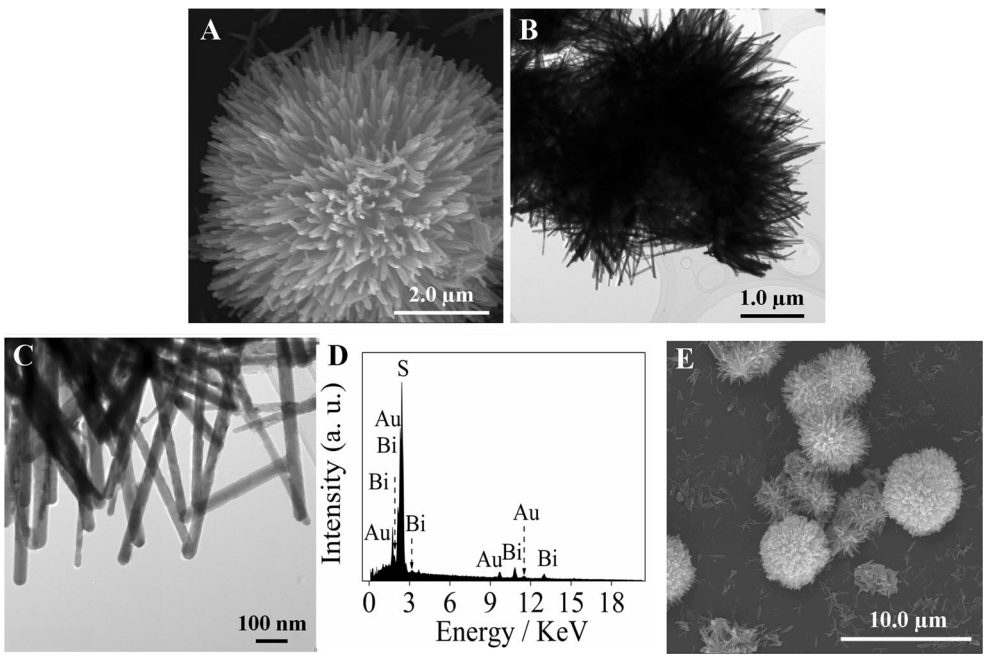

Fig. 1 **a**–**c** SEM, TEM, and high-resolution TEM images of the *d*-Bi_2S_3, respectively. **d** EDX analysis of the *d*-Bi_2S_3. **e** SEM image of Cyt *c*-*d*-Bi_2S_3/CHIT film

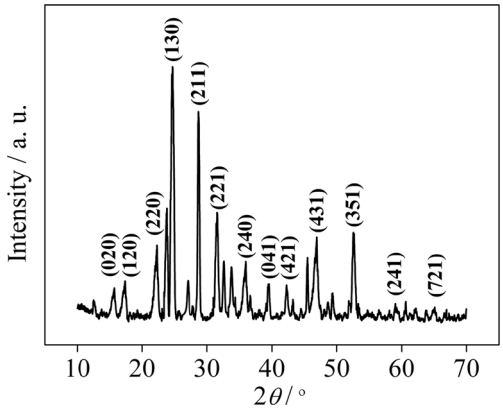

Fig. 2 XRD pattern of d-Bi_2S_3 nanoflower

are very similar and exhibit CD intensity at about 222 and 209 nm that are associated with a corresponding augmentation of α-helix structure, indicating that α-helix conformation is predominant in both of two conditions, although a feeble increase of the CD absorption at 208 nm in curve b in Fig. 3b. Further analysis of these spectral data revealed no significant change in the α-helicity, suggesting that the secondary structure of the proteins remained intact during the course of immobilization [27]. On the other hand, d-Bi_2S_3 does not affect the secondary structure of α-helix, as shown in Fig. 2. The

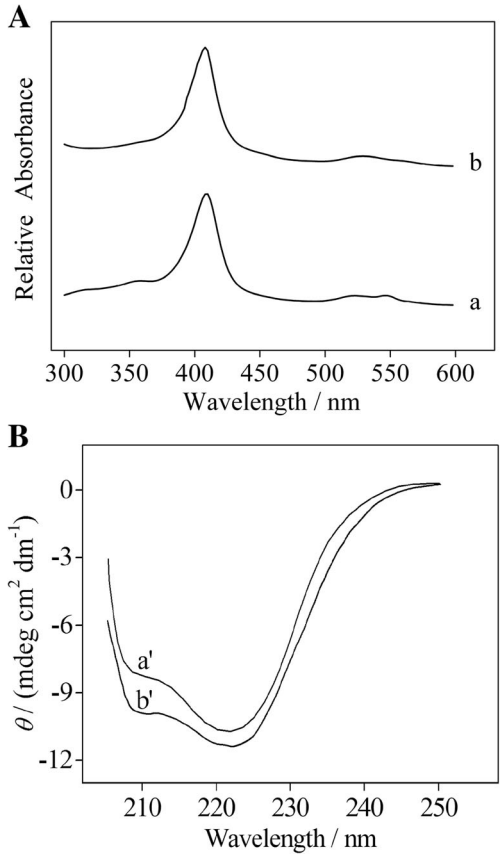

Fig. 3 **a** UV–vis absorption spectra of (*a*) Cyt *c* and (*b*) Cyt *c*-d-Bi_2S_3/CHIT. **b** CD spectra of (*a′*) Cyt *c* and (*b′*) Cyt *c*-d-Bi_2S_3

results were well consistent with the conclusions in electrochemical experiments. All results indicated that d-Bi_2S_3 could essentially maintain the native conformation of Cyt *c*. Thus, d-Bi_2S_3 indeed has good biocompatibility and has well maintained the secondary structure of Cyt *c* in the prepared biosensor.

Direct electrochemistry of Cyt *c*-d-Bi_2S_3/CHIT/GCE

The direct electron transfer of Cyt *c* immobilized in the d-Bi_2S_3/CHIT/GCE was first investigated by cyclic voltammetry. Figure 4 shows the cyclic voltammograms of different electrodes in 0.1 M PBS (pH 7.0) at a scan rate of 50 mV s^{-1}. For the CHIT/GCE (curve a) and d-Bi_2S_3/CHIT/GCE (curve b), no redox peaks can be observed in the potential range from −0.8 to 0.2 V. For the Cyt *c*/CHIT/GCE (curve c), the only one cathodic peak that could be ascribed to the direct electron transfer of Cyt *c* within the composite film is inhibited. However, after immobilization of Cyt *c* together with d-Bi_2S_3 on the CHIT/GC electrode (curve d), a pair of well-defined redox peaks ascribing to the characteristic peaks of the Cyt *c* (Fe^{III}/Fe^{II}) redox couples was observed. The redox peaks imply that the dandelion-like structure of Bi_2S_3 could accelerate the direct electron transfer between Cyt *c* and electrode. The formal potential of the Cyt *c*-d-Bi_2S_3/CHIT/GCE was −0.285 V (vs. SCE), which agrees well with that obtained at a three-dimension porous calcium alginate film-modified electrode [12], and a graphene oxide–carbon nanotube-modified electrode [10] in pH 7.0 buffer solution.

To further investigate the electron transfer process, the cyclic voltammetric responses of the Cyt *c*-d-Bi_2S_3/CHIT/GCE at different scan rates were recorded. As can be seen from Fig. 5a, b, the cathodic and anodic peak currents increase linearly with the increase of scan rates, suggesting a surface-controlled process during the electrochemical reaction. According to the equation $I_p = n^2F^2vA\Gamma/4RT$ [28], the surface coverage (Γ) of Cyt *c* immobilized on the d-Bi_2S_3-modified

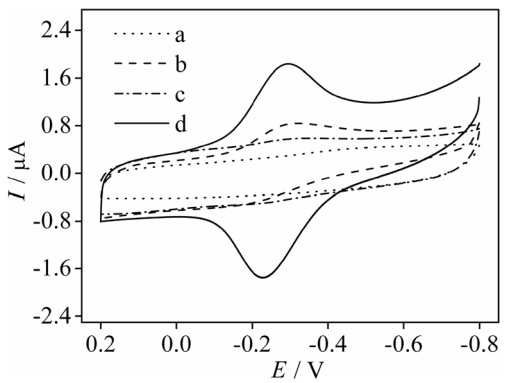

Fig. 4 Cyclic voltammograms of the (*a*) CHIT/GCE, (*b*) d-Bi_2S_3/CHIT/GCE, (*c*) Cyt *c*/CHIT/GCE, and (*d*) Cyt *c*-d-Bi_2S_3/CHIT/GCE in 0.1 M PB solution at a scan rate of 50 mV s^{-1}

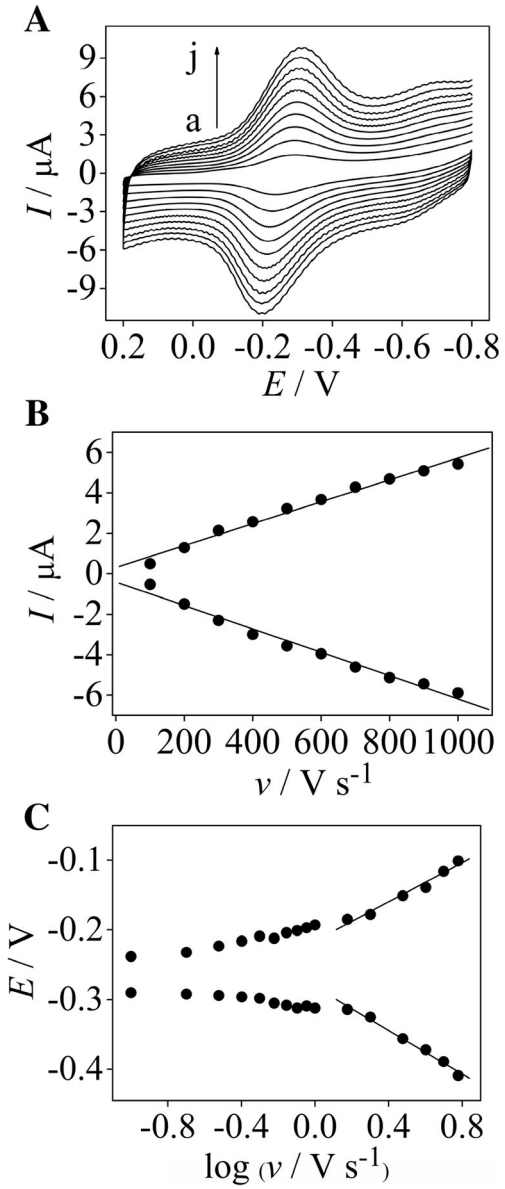

Fig. 5 **a** Cyclic voltammograms of the Cyt *c*-*d*-Bi_2S_3/CHIT/GCE in 0.1 PB solution at various scan rates (from *a* to *j*): 100, 200, 300, 400, 500, 600, 700, 800, 900, and 1000 mV s^{-1}. **b** Plots of peak currents vs. scan rates. **c** Plots of peak potentials vs. logarithm of scan rates

electrode is estimated to be 1.6×10^{-10} mol cm^{-2}, which is higher than the theoretical monolayer coverage (1.4×10^{-12} mol cm^{-2}) [29]. The large surface coverage might result from three-dimensional configuration of the *d*-Bi_2S_3 in which Cyt *c* was immobilized on *d*-Bi_2S_3 film surface. It is generally thinking that the *d*-Bi_2S_3 nanocrystals are composed of Bi_2S_3 nucleus and S^{2-} crust that makes the surface of the *d*-Bi_2S_3 nanocrystals negatively charged. Simultaneously, the selected optimum pH is above the isoelectric points of Cyt *c* (p*I* = 10.2). In this case, Cyt *c* molecules are positively charged. Thus, it could be concluded that the proteins are immobilized onto the *d*-Bi_2S_3 nanocrystals through the electrostatic attractions. At higher scan rate, the values of cathodic and anodic peak potentials were proportional to the logarithm of the scan rates. On the other hand, the oxidation peak shifts to more positive potentials and the reduction peak shifts to more negative potentials. Figure 5c shows the data of peak potentials vs. scan rates. At lower scan rates when $v \leq 1000$ mV s^{-1}, the cathodic and anodic peak potentials changed slightly. While for $v \geq 1000$ mV s^{-1}, the values of cathodic and anodic peak potentials were proportional to the logarithm of the scan rate. In this case, the apparent heterogeneous electron transfer rate constant (k_s) could be calculated based on the Laviron theory. The calculated value of k_s was 13.1 s^{-1}, which was higher or comparable than that were obtained at graphene oxide–carbon nanotube 3.4 s^{-1} [10], poly(diallyldimethylammonium chloride)–graphene nanosheets/gold nanoparticle hybrid nanocomposites 3.14 s^{-1} [30], and comparable at three-dimension scaffold of molecular hydrogels 18.6 s^{-1} [31] as immobilizing matrix, indicating that the Cyt *c* immobilized on the *d*-Bi_2S_3/CHIT composite film achieved a relative fast electron transfer process.

Electrocatalytic properties of Cyt *c*-*d*-Bi_2S_3/CHIT/GCE

It has been shown that Cyt *c* can electrocatalyze the reduction of H_2O_2 with good performances. Thus, the electrocatalytic application of the Cyt *c*-*d*-Bi_2S_3/CHIT/GCE was investigated by cyclic voltammetry. As shown in Fig. 6a, with successive addition of H_2O_2 into the buffer solution, the reduction peak currents of the Cyt *c*-*d*-Bi_2S_3/CHIT/GCE increased dramatically at about −0.3 V. Meanwhile, the oxidation peak currents decreased with an increase of H_2O_2 concentration, demonstrating a typical electrocatalytic reduction process of H_2O_2. Figure 6b shows the catalytic current vs. H_2O_2 concentration was linear in the concentration range 0–3.0 mM with correlation coefficient of 0.9902. Previous investigations have proved that heme proteins react by the Poulos–Kraut mechanism [32] during the electrocatalytic reduction of H_2O_2. Thus, the catalytic procedures can be explained as follows:

$$\left[\text{Cyt } c\left(\text{Fe}^{\text{III}}\right)\right] + H_2O_2 \rightarrow \text{Compound I} + H_2O. \quad (1)$$

$$\text{Compound I} + H_2O_2 \rightarrow \left[\text{Cyt}\, c\left(\text{Fe}^{\text{III}}\right)\right] + H_2O + O_2. \quad (2)$$

$$\left[\text{Cyt } c\left(\text{Fe}^{\text{III}}\right)\right] + H^+ + e^- \rightarrow \left[\text{Cyt}\, c\left(\text{Fe}^{\text{II}}\right)\right] \quad \text{at electrode.} \quad (3)$$

$$\left[\text{Cyt}\, c\left(\text{Fe}^{\text{II}}\right)(+ O_2 \rightarrow)\text{Cyt}\, c\left(\text{Fe}^{\text{II}}\right)\right]\text{–}O_2 \quad \text{fast.} \quad (4)$$

$$\left[\text{Cyt } c\left(\text{Fe}^{\text{II}}\right)\right]\text{–}O_2 + H^+ + e^- \rightarrow \left[\text{Cyt}\, c\left(\text{Fe}^{\text{III}}\right)\right] + H_2O_2 \quad \text{at electrode.} \quad (5)$$

The overall reaction of (1)–(5) would be the following:

$$H_2O_2 + 2H^+ + 2e^- \rightarrow 2H_2O. \quad (6)$$

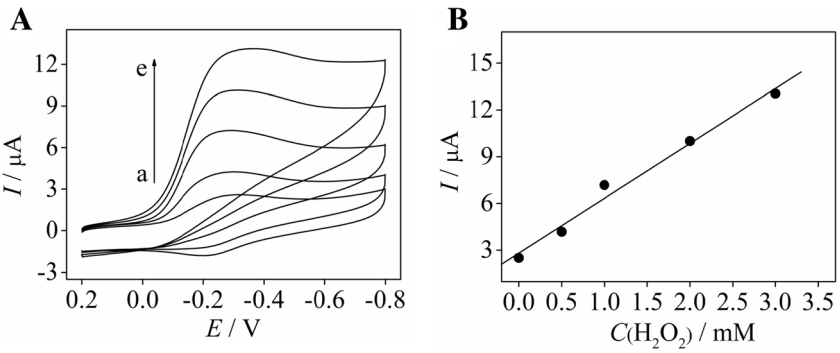

Fig. 6 **a** Cyclic voltammograms of Cyt *c*-*d*-Bi_2S_3/CHIT/GCE in 0.1 M PBS (pH 7.0) in the absence (*a*) and presence of (*b*) 0.5, (*c*) 1.0, (*d*) 2.0, and (*e*) 3.0 mM H_2O_2. **b** Plot of peak current vs. H_2O_2 concentration

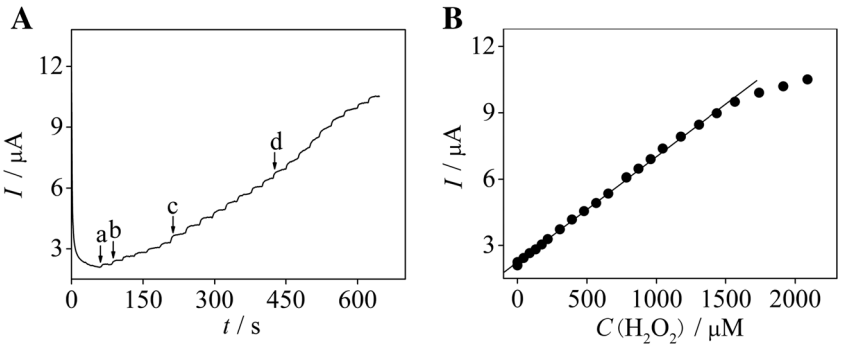

Fig. 7 **a** Amperometric responses of the H_2O_2 biosensor at −0.30 V (vs. SCE) upon successive addition of (*a*) 5 μL 1.0 mM H_2O_2, (*b*) 5, (*c*) 10, and (*d*) 15 μL 87.0 mM H_2O_2 to 10 mL PB solution (0.1 M, pH 7.0). **b** Plot of peak current vs. H_2O_2 concentration

In order to evaluate the performances of the Cyt *c*-*d*-Bi_2S_3/CHIT/GCE for H_2O_2 detection, the amperometric current–time curve was recorded during successively adding H_2O_2 to a continuous stirring PB solution under an applied potential of −0.30 V. As shown from the curve in Fig. 7a, the cathodic reduction currents at about −0.30 V increased linearly with the increasing H_2O_2 concentration. The current responses of Cyt *c*-*d*-Bi_2S_3/CHIT/GCE to H_2O_2 reached a stable plateau within 5 s, suggesting a fast electrode responsive process. The linear range is from 0.5 μM to 1.56 mM with a correlation coefficient of 0.9993 (Fig. 7b). The detection limit is 0.2 μM with the signal-to-noise ratio of 3. Comparison of the analytical performances between Cyt *c*-*d*-Bi_2S_3/CHIT/GCE and other electrodes is shown in Table 1. When the concentration of H_2O_2 is higher than 1.56 mM, the current responses tend to level off, demonstrating typical Michaelis–Menten kinetic characteristic of bioelectrodes based on direct electrochemistry. The apparent Michaelis–Menten constant (K_M^{app}) was estimated to be 40.3 μM according to the electrochemical version of Lineweaver–Burk equation, which was lower than that was obtained at the three-dimension porous calcium alginate film [12], poly(diallyldimethylammonium chloride)–

Table 1 Comparison of analytical performances of some Cyt *c*-based H_2O_2 biosensors

Type of the nanomaterials	k_s (s^{-1})	Linear range (μM)	Detection limit (μM)	K_m (μM)	Ref.
Porous calcium alginate	20.9	1.25–30.0	1.0	61.1	[12]
GO–CNT[b]	3.4	1×10^{-5}–1.4×10^{-4}	2.77×10^{-5}	NA	[10]
PDDA–GE/Au[c]	3.14	10.0–4450.0	2.5	1680.0	[30]
Molecular hydrogels	18.6	0.3–800.0	0.05	NA	[31]
Graphene–*L*-cysteine	NA	0.1 – 480.0	0.015	830.0	[33]
PTCA-GE[a]	NA	5.0–90.0	3.5	NA	[34]
Cyt *c*-*d*-Bi_2S_3/CHIT	13.1	0.5–1560.0	0.2	40.3	This work

NA not applicable

[a] 3,4,9,10-Perylene tetracarboxylic acid functionalized graphene sheets

[b] Graphene oxide–carbon nanotube

[c] Poly(diallyldimethylammonium chloride)–graphene nanosheets/gold nanoparticle hybrid nanocomposites

graphene nanosheets/gold nanoparticle hybrid nanocomposites [30], and graphene–*L*-cysteine [33]. The low value of K_M^{app} implies that Cyt *c* immobilized on the *d*-Bi_2S_3/CHIT film has good affinity to H_2O_2, which could be attributed to large surface-to-volume ratio and good biocompatibility of *d*-Bi_2S_3/CHIT nanocomposite film.

Influences of *d*-Bi_2S_3, CHIT, and film thickness

The effect of *d*-Bi_2S_3 nanoflower amount immobilized within the film is tested by varying different amounts of *d*-Bi_2S_3 nanoflower through preparing composite film-modified electrode process (Fig. 8, white square). Results show that the higher was the *d*-Bi_2S_3 amount, the higher was the peak current, with the maximum signal achieved at 2 mg/mL. The concentration of CHIT was also studied (Fig. 8, white circle). As expected, when varying the CHIT amount from 0.1 to 3.0 mg/mL, the peak currents are increase with the increase of CHIT concentration and achieve the maximum value at 2.0 mg/mL. The above results indicated that higher concentrations of *d*-Bi_2S_3 and CHIT could cause a decrease of the peak current, suggesting that larger amount of *d*-Bi_2S_3 and CHIT could both result in decreased conductivity and mass transportation throughout the film. Thus, 2 mg/mL *d*-Bi_2S_3 and 2.0 mg/mL CHIT were chosen as the optimal amount. The influences of the Cyt *c*-*d*-Bi_2S_3/CHIT film thickness on GCE surface were conducted by varying the Cyt *c*-*d*-Bi_2S_3/CHIT suspension from 2 to 10 μL. Results showed that the maximum response was obtained by using 6 μL of Cyt *c*-*d*-Bi_2S_3/CHIT suspension. Further increase in the amount of Cyt *c*-*d*-Bi_2S_3/CHIT suspension will block the electron transfer and decrease the responding signals for H_2O_2 detection. By using 6 μL of Cyt *c*-*d*-Bi_2S_3/CHIT suspension, the film thickness of the Cyt *c*-*d*-Bi_2S_3/CHIT on GCE surface was about 5.0 μm in a dry state observed by SEM of the vertical section of the film. Thus, 6 μL of suspension is selected to control the thickness of the composite film on electrode surface.

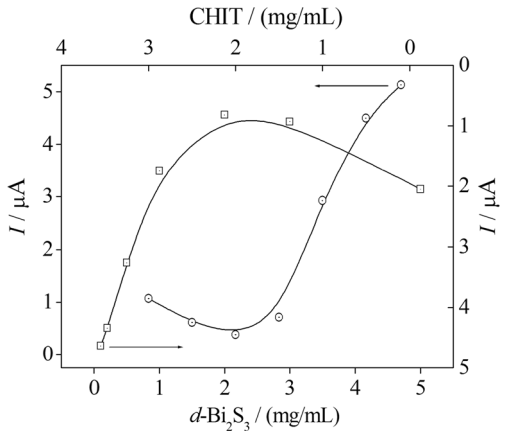

Fig. 8 Influences of the amount of (*white square*) *d*-Bi_2S_3 and the concentration of (*white circle*) CHIT for the immobilization of Cyt *c*

Stability and repeatability of the composite film-modified electrode

The stability of the Cyt *c*-*d*-Bi_2S_3/CHIT/GC electrode is first evaluated by examining the peak currents of Cyt *c* during successive scanning for 100 cycles. It is found that the composite film-modified electrode maintains its 86 % initial activity after 100 cycles. The storage stability of the Cyt *c*-*d*-Bi_2S_3/CHIT/GC electrode is also checked by measuring the current response over a period of 30 days. When not in use, the Cyt *c*-*d*-Bi_2S_3/CHIT/GC electrode is stored dry at 4 °C in a refrigerator. It is found that the Cyt *c*-*d*-Bi_2S_3/CHIT/GC electrode maintains its 85 % initial activity after 20 days. The repeatability and reproducibility of the biosensor were determined. The repeatability of one electrode was conducted by adding 10 μL of 87.0 mM H_2O_2 into a 10 mL 0.1 M PB solution. The relative standard deviation was 5.3 % for six successive assays. Five Cyt *c*-*d*-Bi_2S_3/CHIT/GC electrodes prepared by following identical steps to 10.0 μM H_2O_2 showed a relative standard deviation of 4.7 %, suggesting a good reproducibility of the proposed method.

Conclusions

In summary, the direct electron transfer of Cyt *c* based on *d*-Bi_2S_3 nanoflowers was realized and then a H_2O_2 biosensor was further developed. Cyclic voltammetric results indicated that the *d*-Bi_2S_3 could promote the electron transfer between Cyt *c* and electrode dramatically with a fast electron transfer rate constant of 13.1 s^{-1}. The Cyt *c*-*d*-Bi_2S_3/CHIT/GC electrode also showed excellent electrocatalytic activity toward the reduction of H_2O_2 with lower detection limit and wider response range. It is expected that the biocompatible *d*-Bi_2S_3 materials combined with other redox proteins or biomolecules could serve as a versatile platform for the design of biofuel cells and as electrochemical sensing devices for the determination of H_2O_2 in biological and pharmaceutical samples.

Acknowledgments The authors gratefully acknowledge the financial support of this project by the National Science Fund of China (No. 21275116, 21575113), Specialized Research Fund for the Doctoral Program of Higher Education (No. 20126101110013), the Natural Science Fund of Shaanxi Province in China (No. 2013KJXX-25), and the Scientific Research Foundation of Shaanxi Provincial Key Laboratory (14JS094, 15JS100, and 16JS099).

References

1. Léger C, Bertrand P (2008) Chem Rev 108:2379–2438
2. McGovern RE, Feifel SC, Lisdat F, Crowley PB (2015) Angew Chem Int Ed 54:6356–6359
3. Zhao M, Gao Y, Sun JY, Gao F (2015) Anal Chem 87:2615–2622
4. Li ZJ, Xie C, Wang JH, Meng A, Zhang FH (2015) Sens Actuators B Chem 208:505–511

5. Wang YL, Wang ZC, Rui YP, Li MG (2015) Biosens Bioelectron 64:57–62
6. Baghayeri M, Zare EN, Namadchian M (2013) Sens Actuators B Chem 188:227–234
7. Koposova E, Shumilova G, Ermolenko Y, Kisner A, Offenhausser A, Mourzina Y (2015) Sens Actuators B Chem 207:1045–1052
8. Lata S, Batra B, Karwasra N, Pundir CS (2012) Process Biochem 47:992–998
9. Wang Y, Bian XJ, Liao L, Zhu J, Guo K, Kong JL, Liu BH (2012) Microchim Acta 178:277–283
10. Dinesh B, Mani V, Saraswathi R, Chen SM (2014) RSC Adv 4: 28229–28237
11. Márquez J, Cházaro-Ruiz F, Zimányi L, Palestino G (2014) Electrochim Acta 140:550–556
12. Jian S, Liu XC, Sun H, Hou SF (2014) RSC Adv 4:6165–6172
13. McEntee M, Stevanovic A, Tang WJ, Neurock M, Yates JT Jr (2015) J Am Chem Soc 137:1972–1982
14. Xu XJ, Hu LF, Gao N, Liu SX, Wageh S, Al-Ghamdi AA, Alshahrie A, Fang XS (2015) Adv Funct Mater 25:445–454
15. Wu W, Jiang CZ, Roy VAL (2015) Nanoscale 7:38–58
16. Zeng Y, Li W, Zhang HH, Wu X, Sun W, Zhu ZH, Yu Y (2014) Anal Methods 6:404–409
17. Li J, Yang ZJ, Tang Y, Zhang YC, Hu XY (2013) Biosens Bioelectron 41:698–703
18. Huang FY, Wang F, Feng SQ, Li YJ, Li SX, Li YC (2013) J Solid State Electrochem 17:1295–1301
19. Sun W, Sun ZL, Zhang LQ, Qi XW, Li GJ, Wu J, Wang M (2013) Colloid Surf B Biointerfaces 101:177–182
20. Zhu QH, Gao F, Yang YZ, Zhang B, Wang W, Hu ZS, Wang QX (2015) Sens Actuators B Chem 207:819–826
21. Pan ZQ, Fan H, Shi CG, Bao N, Yu CM, Gu HY (2011) Microchim Acta 173:277–283
22. Butwong N, Zhou L, Moore E, Srijaranai S, Luong JHT, Glennon JD (2014) Electroanalysis 26:2465–2473
23. Meng X, Xu Z, Wang M, Yin H, Ai S (2012) Anal Methods 4: 1736–1741
24. Dong YP, Huang L, Zhang J, Chu XF, Zhang QF (2012) Electrochim Acta 74:189–193
25. Franzen S, Wallace-Williams SE, Shreve AP (2002) J Am Chem Soc 124:7146–7155
26. Barteri M, Gaudiano MC, Rotella S, Benagiano G, Pala A (2000) Biochim Biophys Acta 1479:255–264
27. Zhu L, Wang KQ, Lu TH, Xing W, Li J, Yang XG (2008) J Mol Catal B Enzym 55:93–98
28. Laviron E (1979) J Electroanal Chem 100:263–270
29. Dickerson RE, Takano T, Eisenberg D, Kallai OB, Samson L, Cooper A, Margoliash E (1971) J Biol Chem 246:1511–1535
30. Song YH, Liu HY, Wan LL, Wang Y, Hou HQ, Wang L (2013) Electroanalysis 25:1400–1409
31. Zhou J, Liao CA, Zhang LM, Wang QG, Tian Y (2014) Anal Chem 86:4395–4401
32. D'Antonio J, Ghiladi RA (2011) Biochemistry 50:5999–6011
33. Kong B, Liu W, Li Q, Chen LJ, Liu XY, Zhou JH (2015) Sens Lett 13:267–272
34. Zhang N, Lv XY, Ma WG, Hu YW, Li FH, Han DX, Niu L (2013) Talanta 107:195–202